Available online at www.sciencedirect.com
ScienceDirect
Journal of Nuclear Materials 367–370 (2007) 1197–1202
journal of nuclear materials
www.elsevier.com/locate/jnucmat

The microstructure and strength properties of MA957 nanostructured ferritic alloy joints produced by friction stir and electro-spark deposition welding

P. Miao [a,*], G.R. Odette [a], J. Gould [b], J. Bernath [b], R. Miller [c], M. Alinger [a,d], C. Zanis [c]

[a] Department of Mechanical Engineering, University of California Santa Barbara, Santa Barbara, CA 93106-5080, USA
[b] Edison Welding Institute, 1250 Author E. Adams Dr., Columbus, OH 43221, USA
[c] DDL-OMNI, McLean, VA 22102, USA
[d] University of California Berkeley, Berkeley, CA 94720-1730, USA

Abstract

The nanostructured ferritic alloy (NFA) MA957 was joined by friction stir welding (FSW) and electro-sparked deposition (ESD) welding. Transmission electron microscopy (TEM) and small angle neutron scattering (SANS) characterization studies showed a uniform fine-scale equiaxed ferrite structure with a high dislocation density and slightly coarsened nm-scale particles in the joint region of the FSW weld compared to the base metal. Microhardness and tensile measurements on the FSW showed a modest reduction in the strength of the joint compared to the as-processed MA957. In contrast, the ESD-welds contained considerable porosity and the nm-scale particles dissolved or coarsened significantly, resulting in a larger degradation of the joint region strength. Thus FSW is a promising method for joining NFAs.

1. Introduction

Nanostructured Fe–14Cr–W–Ti–Y_2O_3 dispersion strengthened ferritic alloys (NFAs) have excellent low temperature tensile (>1 GPa), excellent high temperature creep strengths [1–3] and also offer a potential for mitigating radiation damage, including the effects of high helium levels [4,5] in fusion reactor environments. The outstanding properties of NFAs primarily derive from a very high density of Y–Ti–O nm-scale precipitate phases that are formed when powders that are mechanically alloyed (pre-alloyed Fe–14Cr–W–Ti plus Y_2O_3) by milling are subsequently consolidated by hot isostatic pressing (HIPing) or extrusion [5–8]. These phases include small solute clusters rich in Y–Ti and O and slightly larger $Ti_2Y_2O_7$ pyroclore oxides. Therefore, we will refer to these features as nm-scale features (NF) encompassing a size range up to ≈ 8 nm. Thus, a critical issue is producing and maintaining the NF through all stages of processing and fabrication, as well as in high temperature service in irradiation environments.

* Corresponding author. Tel.: +1 805 893 3848; fax: +1 805 893 4731.
E-mail address: p.miao@engineering.ucsb.edu (P. Miao).

0022-3115/$ - see front matter © 2007 Elsevier B.V. All rights reserved.
doi:10.1016/j.jnucmat.2007.03.232

Thus, a major challenge to the use of NFAs is joining. Conventional fusion welding methods are generally not useful, since the NF would be expected to dissolve during typical melting–solidification processes. Joining processes that either avoid melting completely, or that involve very rapid melting and re-solidification, may preserve the NF. In this work we explore two such possible joining methods. FSW is a solid-state joining process that involves mechanical mixing of base metals under severe deformation conditions [9,10]. The material in and near a FSW joint experiences a high temperature cycle, with peak temperatures up to ≈1300–1400 °C, but there is no melting. Thus, FSW may or may not severely damage the NF, and dynamic recrystallization during FSW refines the grains in the stir zone. Furthermore severe deformation induces a high dislocation density [11,12] so that fine-scale FSW microstructures may provide an optimal balance of mechanical properties. ESD welding uses a rapid discharge power source to supply short-duration current pulses to a moving electrode in contact with a substrate [13]. The pulses produce extremely rapid heating, leading to melt droplet formation and deposition in the weld zone as relatively thin splats that cool at very high rates. Thus, the rapid ESD temperature cycle might allow some of the NF to survive in the joint region.

2. Experimental

A commercial MA957 alloy bar of 25 mm (diameter) × 100 mm (length) with a nominal composition of Fe–14 wt%Cr, 0.9% Ti, 0.3% Mo, and 0.25% Y_2O_3 was sectioned into $100 \times 17 \times 2\ mm^3$ and $10 \times 17 \times 2\ mm^3$ slabs for FSW and ESD welding, respectively. FSW butt-welding in the long dimension direction was produced at a tool spindle speed of 130–160 rpm and travel speed of 150–200 mm/min [10]. Other details of the FSW method and tooling are proprietary. The ESD butt-welding was performed with an electrode ground from the MA957 using an Advanced Surfaces and Processes (ASAP) system at a pulse rate of 400 Hz and voltage of 150 V. The butted base metal sections were ground to a ≈ half thickness radius and then filled by the ESD deposit, one side at a time.

The nano-microstructures of the MA957 weld and base metals were characterized by TEM (JEOL2010HR), SANS (NG1 at the National Institute of Standards and Technology) and optical microscopy. Standard 3 mm TEM discs, either centered in the weld region or taken from the base metal, were ground to a thickness of ≈ 0.15 mm and then thinned to electron transparency in a TENUPOL twin-jet electro-polisher with H_2SO_4 + 80%CH_3OH at room temperature. TEM images for the measurement of the NF and larger oxide particles were taken in the same foil orientation (near [0 1 1]) for the MA957 weld and base metals. Details of the experiment, data reduction and analysis for SANS are given elsewhere [14].

The room temperature strength of the FSW and ESD-welded MA957 were evaluated both by microhardness traverses across the weld and tensile tests using subsized flat dogbone specimens with a reduced gauge section in the weld and heat-affected zone transverse to the weld axis. The corresponding tensile tests carried out on the base metal were for the same orientation.

3. Results and discussion

As seen in Fig. 1(a), the MA957 base metal is composed of fine-scale ferrite grains elongated in the extrusion direction. In contrast, as seen in Fig. 1(b), the severe plastic deformation during FSW produces a uniform distribution of fine-scale equiaxed grains, containing a high dislocation density. The optical macro and micrographs in Fig. 2 show that the ESD welding process produces a layered structure, composed of large number of droplet-scale deposits (Fig. 2(a)) along with considerable porosity (the dark features in Fig. 2(b)). Such structures are typical of ESD depositions carried out in air, and clearly do not represent an acceptable joint product. However, the process could be modified to minimize the porosity. Thus the major issue of concern here for the ESD-welds is the fate of the NF with respect to coarsening and/or dissolution.

As seen in the TEM micrographs in Fig. 1(c) and (d), there is a high density of NF in both the base (Fig. 1(c)) and FSW weld (Fig. 1(d)) metals. Based on convergent beam estimates of the foil thickness, the particle size and volume fraction distributions are shown in Fig. 3(a) and (b) and the corresponding NF ($\leqslant$ 8 nm) parameter averages are shown in Table 1.

The TEM on the FSW shows a slight coarsening of the NF, with a nominal increase in the particle diameter from ≈ 3.0 to 3.6 nm and a reduction in number density from ≈ 0.66 to $0.43 \times 10^{23}/m^3$. The larger sizes and smaller number densities of

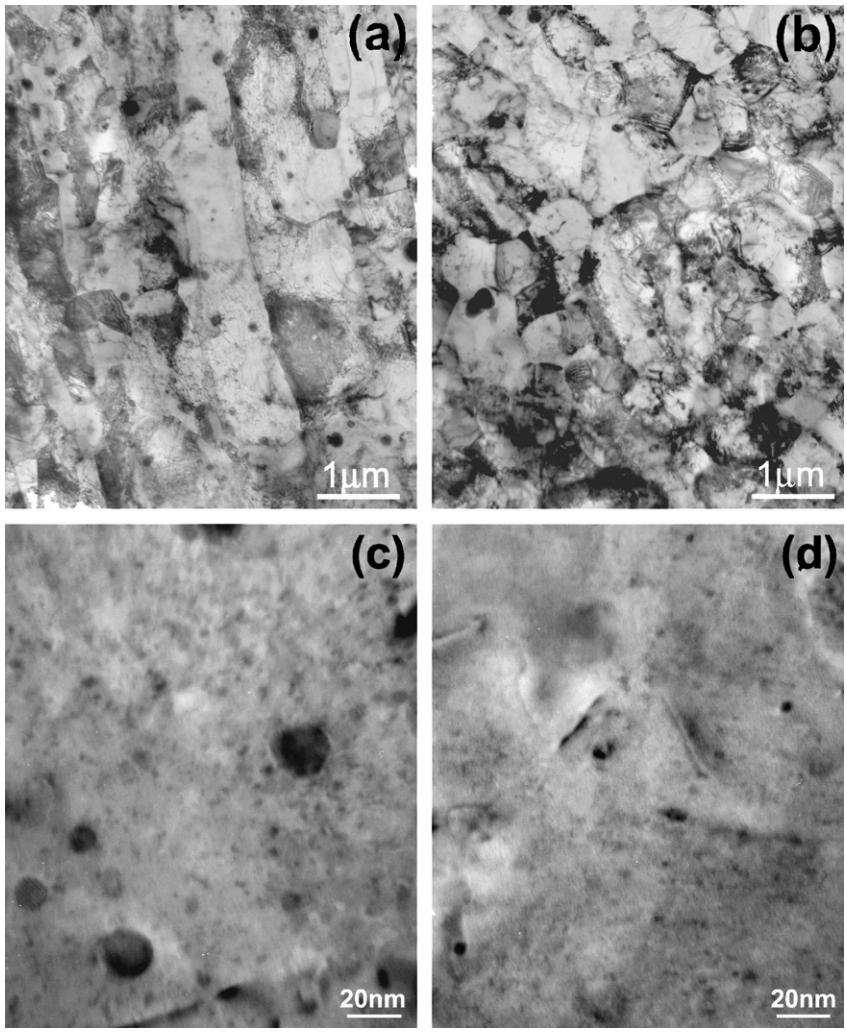

Fig. 1. TEM image of the grain and dislocation microstructure in the MA957 (a) base metal and (b) FSW, and the NF and larger oxide particles in (c) base metal and (d) FSW.

the NF, compared to those from SANS measurement (see Table 1) in this study and TEM results (2.1 nm and $3.9 \times 10^{23}/m^3$ for MA957 baseline) [15] in MA957 aging investigation, are due to the resolution limit in this TEM experiment in which only NFs of $>\approx 2.5$ nm were observed. The volume fraction is approximately constant at $\approx 0.14\%$ (FSW) versus 0.13% (base metal). However, there are two important caveats. First, the smallest NFs ($<\approx 2.5$ nm) were not imaged in TEM. Second the features observed in TEM may include some surface deposit artifacts, e.g. electrolyte residues. Both of these limitations indicate the need for the use of other techniques.

SANS characterization of both the FSW and ESD joints was carried out on the NG1 instrument at NIST. Because of the small size and somewhat irregular shape of the weld specimens, it was not possible to experimentally establish the magnetic to nuclear scattering ratio (M/N) in this case. However, the relative shapes and positions of the SANS curves at 45° to the direction of the magnetic field, shown in Fig. 4, can be qualitatively interpreted to show that FSW decreases the number density and volume fraction and spreads the size distribution of NF. The ESD process has a larger effect, leading to a greater increase in the size and a large reduction in the number density and volume fraction of the NF. The absolute magnitudes of the scattering curves can be estimated assuming a typical $M/N = 1$ for MA957. Corresponding fits to these cross sections, assuming the particles are non-magnetic,

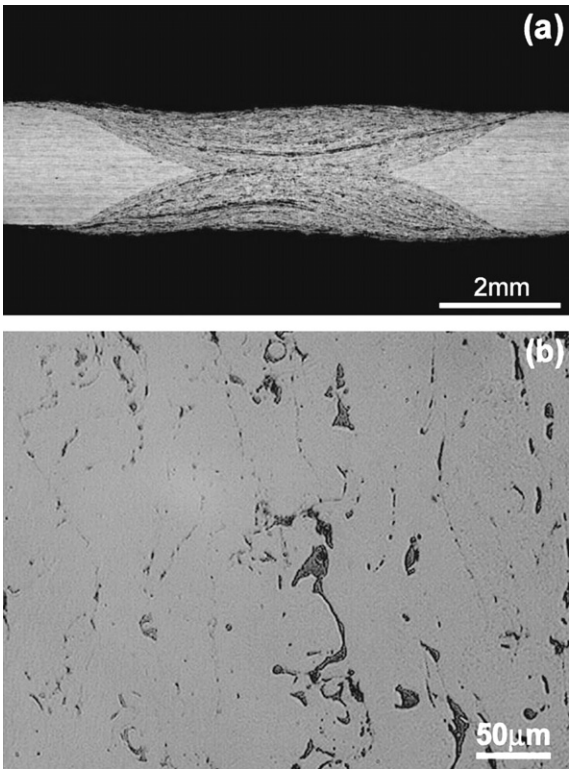

Fig. 2. (a) Macrograph and (b) micrograph (unetched) of the MA957 ESD weld.

Table 1
The average NF (⩽8nm) parameters found in the TEM studies and NF parameters measured by the SANS in the MA957 FSW, ESD and base metal

NF parameters		Base metal	FSW	ESD
Average diameter (nm)	TEM	3.0	3.6	
	SANS	2.4	2.5	4.7
Number density ($\times 10^{23}/m^3$)	TEM	0.66	0.43	
	SANS	8.5	3.5	0.25
Volume fraction (%)	TEM	0.13	0.14	
	SANS	0.6	0.25	0.12

can be used to derive the NF parameters that are summarized in Table 1.

The SANS clearly shows the presence of smaller and more numerous NF compared to TEM. This is expected since: (a) the SANS is optimized to detect small NF features while it is blind to the larger features and (b) TEM does not see the smallest and most numerous NF.

Because of their limitations, neither the SANS nor TEM quantitative results should be taken too literally. However, they are broadly consistent with each other, and show that while FSW reduces the number and volume fraction of NF owing to coarsening and dissolution, the overall effects are relatively modest. In contrast the ESD welding process has a much larger effect on the NF, consistent with a larger reduction in their hardening contribution.

Vicker's diamond pyramid hardness (DPH) traverses at 500 g load across the FSW- and ESD-welds are shown in Fig. 5. Fig. 5(a) for the FSW also includes measurements on a SANS specimen on the weld axis. The strength decreases from the edge of the weld and is a minimum near the center. The average DPH value in the central weld region of the FSW-welded MA957 for various indent

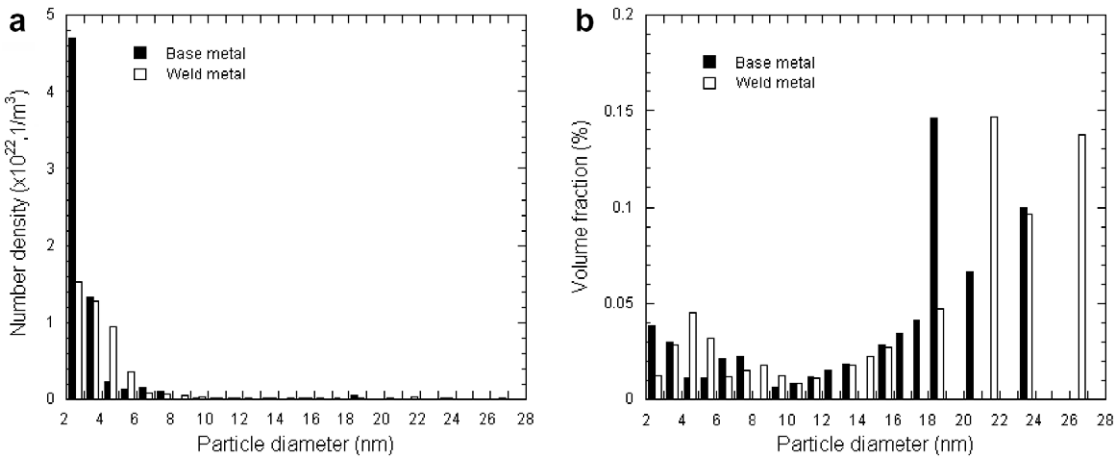

Fig. 3. (a) The number density and (b) the volume fraction of the NF and larger oxide particles in the MA957 FSW and base metal found in the TEM studies.

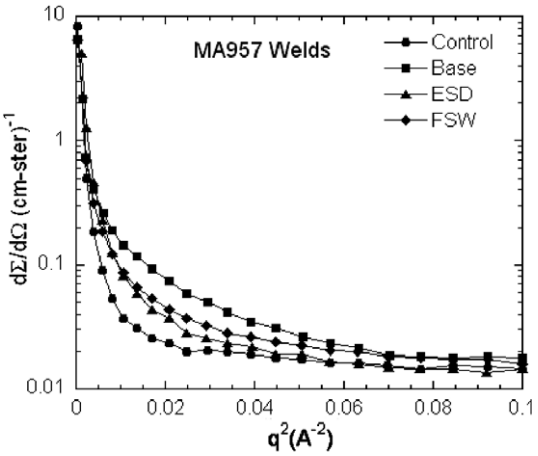

Fig. 4. SANS cross section curves at a 45° angle to the direction of the magnetic field.

sequences was 309 ± 10 kg/mm^2 or about 7% lower than for the base metal value of 332 ± 10 kg/mm^2. In contrast, the average DPH (279 ± 31 kg/mm^2) in the central weld region of the ESD-weld shown in Fig. 5(b) is $\approx 16\%$ lower compared with the base metal.

As shown in Table 2, the ultimate tensile strength (UTS) was decreased by $\approx 9\%$ in the FSW and by $\approx 37\%$ in the ESD-weld. Tensile results for the FSW are consistent with the decrease in hardness in the weakest part of stir zone. The larger decrease in the tensile strength of the ESD-weld, compared to the hardness drop, is probably due to the presence of porosity in this case.

Table 2
UTS of base and weld metal in the FSW- and ESD-welded MA957

Property	Base metal	FSW	ESD
UTS (MPa)	1035 ± 3	942	656[a]

[a] Only one specimen was tested.

4. Discussion

With regard to the key question about the fate of the NF, the SANS results of this study suggest that FSW produces a larger degradation of the smallest NF, but even in this case it is on the order of a 50% reduction in the number density and volume fraction. Somewhat larger NFs are only slightly coarsened. This behavior may be due to a combination of the transient high temperatures during FSW and very severe deformation which results in mechanical dissolution of the small particles by dislocation cutting processes. This conclusion is consistent with the previous observation that small NF is not strong dislocation Orawan-type barriers [14]. Such mechanical cutting may also play a role in the initial mechanical alloying process. The FSW also produces beneficial changes in the microstructure, by refining the grains and making them equiaxed, as well as increasing the dislocation density which contributes the strength of the alloy. The net result is a minimal decrease in the strength of the FSW joint ($< 10\%$). In contrast to the FSW case, the ESD joining process appears to be far less promising. In spite of the rapid sequence of melting and solidification the NFs are severely degraded.

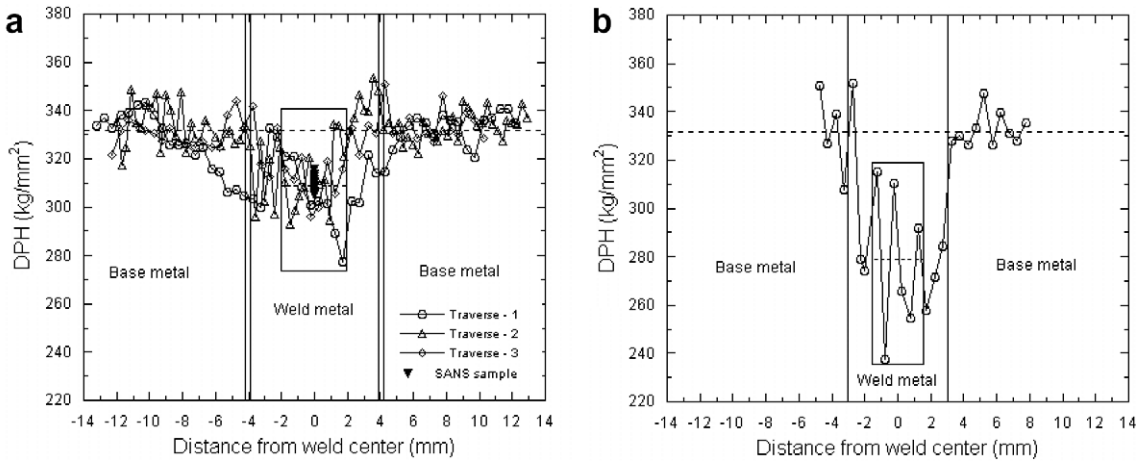

Fig. 5. Microhardness profile across the welds of (a) FSW- and (b) ESD-welded MA957.

It is noted that 'lazy S' was found in the root of the FSW. This defect is caused by the fragmentation of surface oxide layer during the FSW processing, and may degrade mechanical properties (e.g. bending strength). The 'lazy S' may be eliminated or minimized by an increase in heat input during FSW.

5. Summary and conclusions

The FSW produced an attractive high strength joint of MA957 with a uniform fine-scale and equiaxed ferrite structure as well as a high dislocation density in the severely plastically deformed joint stir region. The NF was only slightly degraded during welding in this case. FSW decreased the alloy hardness and ultimate tensile strength by less than 10% compared to the base metal. The ESD MA957 welds contained porosity and the NF were severely degraded during the melting–resolidification process. These microstructural changes resulted in a significant degradation of mechanical properties from ≈16% (hardness) to ≈37% (UTS) compared with the MA957 base metal. Hence, ESD welding does not appear to be a promising method for joining NFA.

Acknowledgements

The authors thank Drs David Gelles and Richard Kurtz of the Pacific Northwest National Laboratory for providing the MA957 used in this study. We also gratefully acknowledge the outstanding support for the SANS experiments provided by the NIST Center for Neutron Research. This research was supported by Small Business Technology Transfer Research (STTR), DOE Office of Fusion Energy Science (Grant #DE-FG03-94ER54275), the NERI DOE Office of Nuclear Energy (Grant #DE-FC07-05ID14663) and the INERI DOE Office of Nuclear Energy through a subcontract with ORNL (Grant #400014112).

References

[1] M.J. Alinger, G.R. Odette, G.E. Lucas, J. Nucl. Mater. 307–311 (2002) 484.
[2] R.L. Klueh, J.P. Shingledecker, R.W. Swindeman, D.T. Hoelzer, J. Nucl. Mater. 341 (2005) 103.
[3] R.L. Klueh, P.J. Maziasz, I.S. Kim, L. Heatherly, D.T. Hoelzer, N. Hashimoto, E.A. Kenik, K. Miyahara, J. Nucl. Mater. 307–311 (2002) 773.
[4] T. Yamamoto et al., J. Nucl. Mater., these Proceedings, doi:10.1016/j.jnucmat.2007.03.047.
[5] M.J. Alinger, G.R. Odette, D.T. Hoelzer, J. Nucl. Mater. 329–333 (2004) 382.
[6] M.K. Miller, D.T. Hoelzer, E.A. Kenik, K.F. Russel, J. Nucl. Mater. 329–333 (2004) 338.
[7] S. Ukai, M. Fujiwara, J. Nucl. Mater. 307–311 (2002) 749.
[8] M. Klimenkov, R. Lindau, A. Möslang, J. Cryst. Growth 249 (2003) 381.
[9] W.M. Thomas, E.D. Nicholas, Mater. Des. 18 (1997) 269.
[10] J. Bernath, J. Gould, Report on Development of Candidate Joining Technology for MA957 Sheet, Edison Welding Institute, Columbus, OH, USA, March, 2005.
[11] Y.S. Sato, T.W. Nelson, C.J. Sterling, R.J. Steel, C.-O. Pettersson, Mater. Sci. Eng. A 397 (2005) 376.
[12] K.V. Jata, K.K. Sankaran, J.J. Ruschau, Metall. Mater. Trans. A 31 (2000) 2181.
[13] G.L. Sheldon, R.N. Johnson, in: K.C. Ludema (Ed.), Wear of Materials, ASME, New York, 1985.
[14] M.J. Alinger, PhD dissertation, University of California Santa Barbara, 2004.
[15] P. Miao, G.R. Odette, T. Yamamoto, M. Alinger, D. Klingensmith, J. Nucl. Mater., submitted for publication.